

# Multi-pulse corona discharges in thunderclouds observed in optical and radio bands

Dongshuai Li<sup>1†</sup>, Alejandro Luque<sup>1</sup>, Nikolai G. Lehtinen<sup>2</sup>, F. J. Gordillo-Vázquez<sup>1</sup>,  
Torsten Neubert<sup>3</sup>, Gaopeng Lu<sup>4</sup>, Olivier Chanrion<sup>3</sup>, Hongbo Zhang<sup>5</sup>, Nikolai Østgaard<sup>2</sup>,  
Víctor Reglero<sup>6</sup>

<sup>1</sup>Instituto de Astrofísica de Andalucía (IAA), CSIC, Granada, Spain.

<sup>2</sup>Birkeland Centre for Space Science, Department of Physics and Technology, University of Bergen, Bergen, Norway.

<sup>3</sup>National Space Institute, Technical University of Denmark (DTU Space), Kongens Lyngby, Denmark.

<sup>4</sup>CAS Key Laboratory of Geospace Environment, University of Science and Technology of China, Hefei, China.

<sup>5</sup>Key Laboratory of Middle Atmosphere and Global Environment Observation (LAGEO),

Institute of Atmospheric Science, Chinese Academy of Sciences, Beijing, China.

<sup>6</sup>Image Processing Laboratory, University of Valencia, Valencia, Spain.

## Key Points:

- Optical multi-pulse corona discharges coincide with Narrow Bipolar Events and their subsequent pulses.
- Subsequent optical pulses are related to horizontally oriented fast breakdowns which emitted faint radio signals.
- The class of horizontally oriented fast breakdowns might play a significant role in the initiation of the lightning leaders.

---

Corresponding author: Dongshuai Li<sup>†</sup> and Alejandro Luque,

Instituto de Astrofísica de Andalucía (IAA), CSIC, Granada, Spain.

<sup>†</sup>Present address: National Space Institute, Technical University of Denmark (DTU Space), Kongens Lyngby, Denmark., (dongshuai@space.dtu.dk, aluque@iaa.es)

## Abstract

How lightning initiates inside thunderclouds remains a major puzzle of atmospheric electricity. By monitoring optical emissions from thunderstorms, the Atmosphere-Space Interactions Monitor (ASIM) onboard the International Space Station is providing new clues about lightning initiation by detecting Blue Luminous Events (BLUEs), which are manifestations of an enigmatic type of electrical discharge that sometimes precedes lightning and is named “fast breakdown”. Here we combine optical and radio observations from a thunderstorm near Malaysia to uncover a new type of event containing multiple optical and radio pulses. We find that the first optical pulse coincides with a strong radio signal in the form of a Narrow Bipolar Event (NBE) but subsequent optical pulses, delayed some milliseconds, have weaker radio signals, possibly because they emanate from a horizontally oriented fast breakdown which does not trigger full-fledged lightning. Our results cast light on the differences between isolated and lightning-initiating fast breakdown.

## Plain Language Summary

One of the biggest mysteries in the atmospheric sciences is to understand how lightning is initiated inside thunderclouds. By combining observations in optical and radio bands, our work uncovers a yet-unreported type of lightning process: multi-pulse corona discharges. For the first time, we cast light on the differences between the isolated and lightning-initiating fast breakdown (an enigmatic type of electrical discharge that is likely present in all lightning initiation events). Our results indicate that there is an unexpected class of horizontally oriented fast breakdown discharges between those that are fully isolated and those that initiate a leader. They have been ignored by all the radio observations so far due to their faint radio signals. However, this would be the class of breakdowns that play a significant role in the initiation of the lightning leaders.

## 1 Introduction

Narrow bipolar events (NBEs) are short, strong radio pulses emitted by thunderclouds (Smith et al., 1999, 2004). Interferometric (Rison et al., 2016) as well as optical, space-based observations (Soler et al., 2020; Li et al., 2021) indicate that their source, with a spatial extent of hundreds of meters to a few kilometers and a duration of some tens of microseconds, is a poorly understood type of electrical breakdown produced by the simultaneous propagation of  $10^8$  to  $10^9$  cold filamentary discharges called streamers (Li et al., 2021; N. Liu et al., 2019; Nijdam et al., 2020). This type of electrical discharge, called fast breakdown, is likely present in all lightning initiation events (Attanasio et al., 2021; Sterpka et al., 2021) and even during flash development, although only under a still undefined set of conditions it is sufficiently strong to manifest itself as an NBE.

NBEs normally occur in isolation (Rison et al., 2016; Kostinskiy et al., 2020) but a small fraction of them, named Initiation-type NBEs (INBEs) (Wu et al., 2014) are the initial event of a lightning flash. Sometimes NBEs are followed by subsequent radio pulses associated with leaders (hot lightning channels); these pulses, sometimes called Initial Breakdown Pulses (IBPs) (e.g., Kostinskiy et al., 2020; Lyu et al., 2019) or Preliminary Breakdown pulses (PBs) (e.g., Kolmašová et al., 2018; Wu et al., 2015), precede by a few milliseconds an intracloud (IC) or cloud-to-ground (CG) lightning discharge. Whereas isolated NBEs are strong emitters of Very High Frequency (VHF) radiation (3000 – 300 000 W) (Rison et al., 2016; Kostinskiy et al., 2020), initiation-type NBEs, even with pulse widths similar to isolated NBEs, present smaller amplitudes and weaker VHF signals (3 – 300 W) (Rison et al., 2016; Kostinskiy et al., 2020; Wu et al., 2014; Bandara et al., 2019).

Most of this knowledge about NBEs and fast breakdown derives from radio observations but these have been recently complemented by optical detections from space. The Modular Multispectral Imaging Array (MMIA) instrument of the Atmosphere-Space Interactions Monitor (ASIM), operating since 2018 from the International Space Station (ISS), has detected a large number of Blue Luminous Events (BLUEs) globally (Soler et al., 2021), which are optical pulses with a strong 337 nm signal, associated with streamer discharges, but lacking the 777 nm emissions that would indicate the presence of a hot leader (Soler et al., 2020; Li et al., 2021; F. Liu, Lu, et al., 2021).

69 Combined radio and optical studies provide strong evidence that every NBE has a BLUE counterpart  
 70 (Soler et al., 2020; Li et al., 2021; F. Liu, Lu, et al., 2021). Hence BLUES are another manifestation  
 71 of fast breakdown.

72 Novel optical observations help to elucidate the context in which fast breakdown occurs. Soler  
 73 et al. (2020) found that a significant fraction of BLUES contained more than one optical pulse  
 74 with a delay between pulses of a few milliseconds. Here we combine observations from MMIA  
 75 and from ground-based Very Low Frequency/Low Frequency (VLF/LF) radio sensors to investigate  
 76 a number of multi-pulse BLUES from a thunderstorm near Malaysia. We find that in all these  
 77 events the first optical pulse has an unambiguous NBE counterpart. Remarkably, we also find that  
 78 the subsequent optical pulses, even though they have optical amplitudes comparable to the leading  
 79 pulse, are accompanied by faint, sometimes undetectable, radio emissions. The implication is that  
 80 NBEs are frequently followed by a new type of event that has escaped detection until now. Our  
 81 observations are compatible with these events being horizontally directed fast breakdown which  
 82 does not initiate a leader.

## 83 2 Instruments and Observations

84 Since its commissioning in 2018, the Modular Multispectral Imaging Array (MMIA) of the  
 85 Atmosphere-Space Interactions Monitor (ASIM) has been observing Earth thunderstorms from space  
 86 in a nadir-viewing geometry from the International Space Station (ISS) (Chanrion et al., 2019; Neu-  
 87 bert et al., 2019). MMIA contains three photometers with a sampling rate of 100 ksamples/s: one  
 88 photometer in the ultraviolet (UV) band at 180-230 nm, one in the near-UV at the strongest spectral  
 89 line of the nitrogen second positive system (337 nm) and one at the strongest lightning emission  
 90 band (777.4 nm). The last two photometers are complemented with cameras sensitive to the same  
 91 wavelengths. The spatial resolution of the cameras on the ground is around  $400\text{ m} \times 400\text{ m}$  and they  
 92 have an integration time of 83.3 ms.

93 Our radio-frequency data comes from a broadband Very Low Frequency/Low Frequency (VLF/LF)  
 94 magnetic sensor that operates at 400 Hz to 400 kHz and is located at Universiti Teknikal Malaysia  
 95 Melaka (UTeM), Malacca, Malaysia (Zhang et al., 2016; Ahmad et al., 2017). To compare MMIA  
 96 and VLF/LF data correcting for MMIA's time uncertainty we matched MMIA pulses with data from  
 97 the GLD360 lightning detection network (Said & Murphy, 2016), obtaining a time shift for MMIA  
 98 with respect to the ground-based VLF/LF measurements of  $(-15.00 \pm 0.65)$  ms (see Figure S1 in  
 99 Supplemental Material).

100 On the evening of April 30, 2020, there were 16 Blue LUMinous Events (BLUES) simultane-  
 101 ously observed by the 337 nm photometer and its filtered camera of MMIA, as well as the ground-  
 102 based VLF/LF sensor near Malaysia (Ahmad et al., 2017), with absent or negligible signals in both  
 103 the 180 - 230 nm photometer and in the 777.4 nm photometer and filtered camera. Among the events,  
 104 there are 8 single-pulse BLUES (Soler et al., 2020; Li et al., 2021) and 8 multiple-pulse BLUES. We  
 105 focus mainly on the multiple-pulse BLUES.

106 To illustrate the thunderstorm context of the BLUES, figure 1 shows the distribution of intr-  
 107 acloud (IC)/cloud-to-ground (CG) lightning with the 8 multi-pulsed BLUES superimposed on the  
 108 cloud Top Blackbody Brightness Temperature (TBB, given in Kelvin) provided by the Himawari-8  
 109 satellite (Bessho et al., 2016) in ten-minute intervals starting at 17:40:00 UTC, 17:50:00 UTC and  
 110 18:00:00 UTC. Because GLD360 only captured 3 events, we determine the locations of multiple-  
 111 pulse BLUES by projecting the brightest pixel of the of 337-nm camera images into geo-coordinates  
 112 (latitude and longitude). We also show the GLD360-detected lightning flashes surrounding our  
 113 events, including their classification as positive or negative, CG or IC. The BLUES, which occurred  
 114 in the time period from 17:50:00 to 17:51:00 UTC, are accompanied by the highest concentration of  
 115 IC and CG lightning with an apparent decrease of the negative CG flash rate.

116 The detailed features of all multiple-pulse BLUES are listed in Table 1. As an example, the  
 117 multiple-pulse BLUE with ID 1 is presented in Figure 2, with other cases given in Figure S2-S9 in  
 118 the Supplemental Material. The multiple-pulse BLUES include one primary BLUE pulse and one

119 or several subsequent BLUE pulses within 1 ms to 9 ms. In most cases, both rise time and time  
 120 duration of the subsequent BLUE pulses are found to be similar or somewhat shorter than those  
 121 corresponding to the primary BLUES; the irradiances of the primary BLUES are higher than those  
 122 of the subsequent BLUES pulses by about a factor of two. All the BLUES are isolated from other  
 123 IC or CG lightning discharges detected by either GLD360 or the 777.4 nm photometer and filtered  
 124 camera of MMIA within at least 100 ms. That means that they do not initiate any leader activity and  
 125 therefore would be classified as isolated NBEs.

### 126 3 Results

127 As shown in Figure 2 and Figures S2-S9 in the Supplemental Material, all the multiple-pulse  
 128 BLUES are associated with an isolated positive NBE sometimes accompanied by faint subsequent  
 129 radio pulse trains. Figure 3 demonstrate the correlation of the horizontal  $B$  fields ( $B_{EW}$  and  $B_{NS}$ ) for  
 130 both the positive NBE and its subsequent pulses for event 1 (See Figures S11-S19 in Supplemental  
 131 Materials for other cases).

132 As shown in figure 3(d), the NBE pulses exhibit a tight linear relationship of the horizontal  
 133  $B$  fields, something that is expected for the horizontally propagating ground wave of a vertical dis-  
 134 charge. However, in the subsequent pulses the horizontal components of the field trace elliptical  
 135 curves (see Figure 3(h)). As this is a projection into the horizontal plane of the trajectory of the  
 136 magnetic field in the plane perpendicular to the wave propagation, the implication is that the wave  
 137 is elliptically polarized. One explanation for this behaviour is that the electric current responsible  
 138 for the subsequent pulses is oriented horizontally: in that case the ground wave is absent and the  
 139 first signal to reach the detector is the wave reflected in the ionosphere. Due to the anisotropy intro-  
 140 duced by the geomagnetic field, different components of the wave electromagnetic fields propagate  
 141 differently in the magnetized plasma of the lower ionosphere, introducing a phase shift between dif-  
 142 ferent components. This would explain both the weak amplitude and the elliptical polarization of  
 143 the observed signal.

144 We tested this hypothesis by means of a Full Wave Method (FWM) electromagnetic model  
 145 (Lehtinen & Inan, 2008, 2009) (see Methodology in Supplemental Material for further details).  
 146 We simulated the signals produced by both vertical and horizontal dipole current sources imitating  
 147 the event-detector geometry of our observations. The results, shown in figure 3, reproduce the  
 148 qualitative features of the waveform measured by the ground-based VLF/LF. For the case of NBE,  
 149 both ground wave and its first and second reflected sky waves can be clearly seen in figure 3(a, c)  
 150 with a linear relationship between the magnetic field components  $B_x$  and  $B_y$  (see figure 3(b, d)). For  
 151 the subsequent pulse trains, the ground wave is absent and the magnetic field components  $B_x$  and  
 152  $B_y$  of the first and second sky waves trace elliptical curves (see figure 3(e,f,g,h)). These simulations  
 153 support our hypothesis of a horizontal discharge triggered by the primary, vertical fast breakdown  
 154 that generates the NBE.

155 To better understand the multiple-pulse BLUES, we simulated the propagation of their opti-  
 156 cal emissions within the thundercloud with both an analytical diffusion model and a Monte Carlo  
 157 model (Li et al., 2020) (see Methodology in Supplemental Material for further details). Table 2  
 158 lists the inferred parameters of the multiple-pulse BLUES. The estimated depths  $L$  (relative to the  
 159 cloud top) of the BLUES are derived by the analytical diffusion model based on the 337-nm pho-  
 160 tometer signals of MMIA, assuming a cloud particle radius  $r = 20 \mu\text{m}$  and droplet number density  
 161  $N_d = 10^8 \text{ m}^{-3}$  to  $3 \times 10^8 \text{ m}^{-3}$ . The altitudes  $H$  of the NBEs are evaluated based on the ground-based  
 162 VLF/LF radio signals by using the simplified ray-theory method (Smith et al., 1999, 2004), which  
 163 involves an uncertainty of about  $\pm 1 \text{ km}$  (Li et al., 2020).

164 We see in Table 2 that the positive NBEs are located at relatively high altitudes with  $H =$   
 165  $16 \text{ km}$  to  $18 \text{ km}$ , which are above the median heights of the majority of positive NBEs (about  $13 \text{ km}$ )  
 166 reported in the literature (Smith et al., 2004; Wu et al., 2014; F. Liu, Zhu, et al., 2021). This suggests  
 167 that the occurrence of multi-pulsed BLUE events may be related to the rare occurrence of high-  
 168 altitude positive NBEs (Wu et al., 2014). As shown in Table 2, our modeling indicates that the

169 subsequent BLUE pulses are located at similar or slightly higher altitudes than the primary BLUEs,  
 170 with a depth of  $L = 1 \text{ km to } 3 \text{ km}$  measured from the cloud top. This low depth explains why MMIA  
 171 not only detects the primary BLUEs but also their subsequent BLUE pulses. The optical energy  
 172 in the 337-nm band emitted by fast breakdown of the primary NBE is about  $10^3 \text{ J}$ , which involves  
 173 around  $10^8$  streamer branching events evaluated as discussed by Li et al. (2021). The ratio of the  
 174 irradiances and the streamer branches is expected to have a roughly linear relationship, thus the  
 175 secondary BLUEs involve about  $5 \times 10^7$  streamer breaching events.

176 We can shed some light into what differentiates multiple-pulse from single-pulse BLUEs by  
 177 looking at the electrical currents of the fast breakdown where they originate. We estimated the  
 178 current moments ( $M_i$ ) of all the 16 BLUEs with sufficient data in the investigated thunderstorm,  
 179 including the 8 multiple-pulse BLUEs and the 8 single-pulse BLUEs. Starting from the azimuthal  
 180 magnetic field component,  $B_\phi$ , we solved the inverse convolution problem using the Uman's equa-  
 181 tion (Uman et al., 1975) shown in (see Methodology and Figure S10 in the Supplemental Material  
 182 for further details). Figure 4 shows a linear relationship between the amplitude of the azimuthal  
 183 magnetic field component  $B_\phi$  and the estimated current moment  $M_i$ . Despite one outlier far from the  
 184 other multiple-pulse BLUEs with ID 7, all the single-pulse and multiple-pulse BLUEs are well sep-  
 185 arated into two clusters. The primary BLUEs of the multiple-pulse BLUEs have relatively weaker  
 186 current moments and amplitudes than those corresponding to the single-pulse BLUEs. This is rem-  
 187 iniscent of initiation-type NBEs, which also have weaker source currents. We emphasize however  
 188 that all the multiple-pulse NBEs that we analyzed are isolated NBEs, separated from any IC or CG  
 189 lightning discharges detected by either GLD360 or the 777.4-nm band of MMIA within at least  
 190 100 ms. They are also located at relatively high altitudes nearby cloud tops, unlike the INBEs nor-  
 191 mally located deeply inside the thundercloud (Smith et al., 2004; Wu et al., 2014).

#### 192 4 Discussion and conclusions

193 Our results suggest that a fraction of so-called isolated NBEs, which do not initiate leader  
 194 activity and are therefore not the starting event of a lightning flash, nevertheless trigger subsequent  
 195 fast breakdown activity. We now discuss some implications of these findings.

196 Turning first to the thunderstorm environment that surrounds the analyzed multiple-pulse BLUEs,  
 197 we notice from the lightning distribution in Figure 1 that the rate of negative CGs exceeds that of  
 198 positive ones by about a factor three, which suggests that the thunderstorm has a dipole-like elec-  
 199 trical structure with the positive charge above the negative charge (Wilson, 1956). However, the  
 200 charge structures can be more complex in the convective region of the thunderstorm (Stolzenburg et  
 201 al., 1998). Both IC and CG flash rates vary dramatically during the time interval when the BLUEs  
 202 occurred.

203 The negative CG rate decreases sharply as the rate of the positive ICs increases, and later the  
 204 rates of all ICs and CGs start to increase. The dramatic change of the lightning rates suggests that the  
 205 lightning discharges are produced inside a thunderstorm with deep convective updrafts (Wiens et al.,  
 206 2005; Petersen & Rutledge, 1998). The ring structures shown in Figure S5 and S7 further illustrate  
 207 that there is a cloud turret extending above the cloud top surface during the occurrence interval of  
 208 the BLUEs (Luque et al., 2020). One hypothesis for this is that the positive NBEs are produced  
 209 between the positive charge lifted to relatively high altitude by the strong updraft and the negative  
 210 screening charge layer which lies close to the overshooting region of the cloud (MacGorman et al.,  
 211 2017).

212 Our results are connected to the problem of lightning initiation and the nature of fast break-  
 213 down. If our interpretation is correct, there is an intermediate class of fast breakdown discharges  
 214 between those that are fully isolated and those that initiate a leader. This would be the class of break-  
 215 downs that trigger subsequent discharges which do not promote to leaders. It is unclear whether  
 216 these discharges, with a primarily horizontal orientation and associated with faint radio pulses, are  
 217 similar to the primarily vertical fast breakdown events described previously in the literature (Rison  
 218 et al., 2016; Tilles et al., 2019; Lyu et al., 2019; N. Y. Liu & Dwyer, 2020; Huang et al., 2021). It

219 is also unknown whether NBE-initiated leaders are initiated by horizontal fast breakdown. These  
 220 questions should be addressed by future research.

## 221 Acknowledgments

222 The authors would like to thank Dr. Mohd Riduan Ahmad at Universiti Teknikal Malaysia  
 223 Melaka (UTEM) for his cooperation on the VLF/LF sferics at Melaka station. This work was sup-  
 224 ported by the European Research Council (ERC) under the European Union H2020 programme/ERC  
 225 grant agreement 681257. It also received funding from the European Union Horizon 2020 research  
 226 and innovation programme under the Marie Skłodowska-Curie grant agreement SAINT 722337.  
 227 Additionally, this work was supported by the Spanish Ministry of Science and Innovation, MINECO,  
 228 under the project PID2019-109269RB-C43 and FEDER program. D.L., A.L. and F.J.G.V. acknowl-  
 229 edge financial support from the State Agency for Research of the Spanish MCIU through the “Center  
 230 of Excellence Severo Ochoa” award for the Instituto de Astrofísica de Andalucía (SEV-2017-0709).

## 231 Open Research

232 The Modular Multispectral Imaging Array (MMIA) level 1 data is proprietary and not cur-  
 233 rently available for public release. Interested parties should direct their request to the ASIM Facility  
 234 Science Team (FST). ASIM data request can be submitted through: <https://asdc.space.dtu.dk> by  
 235 sending a message to the electronic address [asdc@space.dtu.dk](mailto:asdc@space.dtu.dk). The Himawari-8 gridded data in  
 236 this study is public to the registered users and supplied by the P-Tree System, Japan Aerospace Ex-  
 237 ploration Agency (JAXA)/Earth Observation Research Center (EORC) ([https://www.eorc.jaxa](https://www.eorc.jaxa.jp/ptree/)  
 238 [.jp/ptree/](https://www.eorc.jaxa.jp/ptree/)). The data that support the findings of this study are openly available in [https://](https://doi.org/10.5281/zenodo.6123813)  
 239 [doi.org/10.5281/zenodo.6123813](https://doi.org/10.5281/zenodo.6123813). The Cloudscat Monte Carlo simulation code (Luque et al.,  
 240 2020) is available at <https://github.com/aluque/CloudScat.jl>. The stanford Full-Wave  
 241 Method (StanfordFWM) code (Lehtinen & Inan, 2008, 2009) is available at [https://gitlab](https://gitlab.com/nleht/stanfordfwm/)  
 242 [.com/nleht/stanfordfwm/](https://gitlab.com/nleht/stanfordfwm/).

## 243 References

- 244 Ahmad, M. R., Periannan, D., Sabri, M. H. M., Aziz, M. Z. A. A., Lu, G., Zhang, H., ... Cooray, V.  
 245 (2017). Emission heights of narrow bipolar events in a tropical storm over the Malacca Strait. In  
 246 *2017 international conference on electrical engineering and computer science (icecos)* (p. 305-  
 247 309). doi: <https://doi.org/10.1109/ICECOS.2017.8167155>
- 248 Attanasio, A., da Silva, C., & Krehbiel, P. (2021). Electrostatic conditions that produce  
 249 fast breakdown in thunderstorms. *Journal of Geophysical Research: Atmospheres*, *126*(19),  
 250 e2021JD034829. (e2021JD034829 2021JD034829) doi: <https://doi.org/10.1029/2021JD034829>
- 251 Bandara, S., Marshall, T., Karunarathne, S., Karunarathne, N., Siedlecki, R., & Stolzenburg, M.  
 252 (2019). Characterizing three types of negative narrow bipolar events in thunderstorms. *Atmo-*  
 253 *spheric Research*, *227*, 263-279. doi: <https://doi.org/10.1016/j.atmosres.2019.05.013>
- 254 Bessho, K., Date, K., Hayashi, M., Ikeda, A., Imai, T., Inoue, H., ... others (2016). An introduction  
 255 to Himawari-8/9—Japan’s new-generation geostationary meteorological satellites. *Journal of the*  
 256 *Meteorological Society of Japan. Ser. II*, *94*(2), 151–183. doi: <https://doi.org/10.2151/jmsj.2016>  
 257 -009
- 258 Chanrion, O., Neubert, T., Rasmussen, I. L., Stoltze, C., Tcherniak, D., Jessen, N. C., ... oth-  
 259 ers (2019). The modular multispectral imaging array (MMIA) of the ASIM payload on the  
 260 international space station. *Space Science Reviews*, *215*(4), 1–25. doi: [https://doi.org/10.1007/](https://doi.org/10.1007/s11214-019-0593-y)  
 261 [s11214-019-0593-y](https://doi.org/10.1007/s11214-019-0593-y)
- 262 Huang, A., Cummer, S. A., & Pu, Y. (2021). Lightning Initiation from Fast Negative Break-  
 263 down is Led by Positive Polarity Dominated Streamers. *Geophysical Research Letters*, *48*,  
 264 e2020GL091553. doi: [10.1029/2020GL091553](https://doi.org/10.1029/2020GL091553)
- 265 Kolmašová, I., Santolík, O., Defer, E., Rison, W., Coquillat, S., Pedebay, S., ... Pont, V. (2018,  
 266 February). Lightning initiation: Strong pulses of VHF radiation accompany preliminary break-

- 267 down. *Scientific Reports*, 8, 3650. doi: <https://doi.org/10.1038/s41598-018-21972-z>
- 268 Kostinskiy, A. Y., Marshall, T. C., & Stolzenburg, M. (2020). The mechanism of the origin  
269 and development of lightning from initiating event to initial breakdown pulses (v.2). *Journal*  
270 *of Geophysical Research: Atmospheres*, 125(22), e2020JD033191. doi: [https://doi.org/10.1029/](https://doi.org/10.1029/2020JD033191)  
271 2020JD033191
- 272 Lehtinen, N. G., & Inan, U. S. (2008). Radiation of elf/vlf waves by harmonically varying cur-  
273 rents into a stratified ionosphere with application to radiation by a modulated electrojet. *Jour-*  
274 *nal of Geophysical Research: Space Physics*, 113(A6), A06301. doi: [https://doi.org/10.1029/](https://doi.org/10.1029/2007JA012911)  
275 2007JA012911
- 276 Lehtinen, N. G., & Inan, U. S. (2009). Full-wave modeling of transionospheric propagation  
277 of vlf waves. *Geophysical Research Letters*, 36(3), L03104. doi: [https://doi.org/10.1029/](https://doi.org/10.1029/2008GL036535)  
278 2008GL036535
- 279 Li, D., Liu, F., Pérez-Invernón, F. J., Lu, G., Qin, Z., Zhu, B., & Luque, A. (2020). On the accuracy  
280 of ray-theory methods to determine the altitudes of intracloud electric discharges and ionospheric  
281 reflections: Application to narrow bipolar events. *Journal of Geophysical Research: Atmospheres*,  
282 125(9), e2019JD032099. doi: <https://doi.org/10.1029/2019JD032099>
- 283 Li, D., Luque, A., Gordillo-Vázquez, F. J., Liu, F., Lu, G., Neubert, T., ... Reglero, V. (2021).  
284 Blue Flashes as Counterparts to Narrow Bipolar Events: The Optical Signal of Shallow In-Cloud  
285 Discharges. *Journal of Geophysical Research: Atmospheres*, 126(13), e2021JD035013. doi:  
286 10.1029/2021JD035013
- 287 Liu, F., Lu, G., Neubert, T., Lei, J., Chanrion, O., Østgaard, N., ... Zhu, B. (2021). Optical emissions  
288 associated with narrow bipolar events from thunderstorm clouds penetrating into the stratosphere.  
289 *Nature Communications*, 12(6631). doi: <https://doi.org/10.1038/s41467-021-26914-4>
- 290 Liu, F., Zhu, B., Lu, G., Lei, J., Shao, J., Chen, Y., ... Zhou, H. (2021). Meteorological and electrical  
291 conditions of two mid-latitude thunderstorms producing blue discharges. *Journal of Geophysical*  
292 *Research: Atmospheres*, 126(8), e2020JD033648. doi: <https://doi.org/10.1029/2020JD033648>
- 293 Liu, N., Dwyer, J. R., Tilles, J. N., Stanley, M. A., Krehbiel, P. R., Rison, W., ... Wilson, J. G.  
294 (2019). Understanding the radio spectrum of thunderstorm narrow bipolar events. *Journal of*  
295 *Geophysical Research: Atmospheres*, 124(17-18), 10134-10153. doi: [https://doi.org/10.1029/](https://doi.org/10.1029/2019JD030439)  
296 2019JD030439
- 297 Liu, N. Y., & Dwyer, J. R. (2020). Thunderstorm high-frequency radio bursts with weak low-  
298 frequency radiation. *Geophysical Research Letters*, 47(23), e2020GL090325. doi: [https://doi.org/](https://doi.org/10.1029/2020GL090325)  
299 10.1029/2020GL090325
- 300 Luque, A., Gordillo-Vázquez, F. J., Li, D., Malagón-Romero, A., Pérez-Invernón, F. J.,  
301 Schmalzried, A., ... Østgaard, N. (2020). Modeling lightning observations from space-  
302 based platforms (Cloudscat.jl 1.0). *Geoscientific Model Development*, 13(11), 5549–5566. doi:  
303 <https://doi.org/10.5194/gmd-13-5549-2020>
- 304 Lyu, F., Cummer, S. A., Qin, Z., & Chen, M. (2019). Lightning initiation processes imaged with  
305 very high frequency broadband interferometry. *Journal of Geophysical Research: Atmospheres*,  
306 124(6), 2994-3004. doi: <https://doi.org/10.1029/2018JD029817>
- 307 MacGorman, D. R., Elliott, M. S., & DiGangi, E. (2017). Electrical discharges in the overshooting  
308 tops of thunderstorms. *Journal of Geophysical Research: Atmospheres*, 122(5), 2929-2957. doi:  
309 <https://doi.org/10.1002/2016JD025933>
- 310 Neubert, T., Østgaard, N., Reglero, V., Blanc, E., Chanrion, O., Oxborrow, C. A., ... Bhanderi,  
311 D. D. (2019). The ASIM mission on the international space station. *Space Science Reviews*,  
312 215(2), 1–17. doi: <https://doi.org/10.1007/s11214-019-0592-z>
- 313 Nijdam, S., Teunissen, J., & Ebert, U. (2020, nov). The physics of streamer discharge phenomena.  
314 *Plasma Sources Science and Technology*, 29(10), 103001. doi: 10.1088/1361-6595/abaa05
- 315 Petersen, W. A., & Rutledge, S. A. (1998). On the relationship between cloud-to-ground lightning  
316 and convective rainfall. *Journal of Geophysical Research: Atmospheres*, 103(D12), 14025-14040.  
317 doi: <https://doi.org/10.1029/97JD02064>
- 318 Rison, W., Krehbiel, P. R., Stock, M. G., Edens, H. E., Shao, X.-M., Thomas, R. J., ... Zhang, Y.  
319 (2016). Observations of narrow bipolar events reveal how lightning is initiated in thunderstorms.  
320 *Nature communications*, 7, 10721. doi: 10.1038/ncomms10721(2016)

- 321 Said, R., & Murphy, M. (2016). GLD360 upgrade: Performance analysis and applications. In *24th*  
322 *international lightning detection conference*.
- 323 Smith, D. A., Heavner, M. J., Jacobson, A. R., Shao, X. M., Massey, R. S., Sheldon, R. J., &  
324 Wiens, K. C. (2004). A method for determining intracloud lightning and ionospheric heights  
325 from VLF/LF electric field records. *Radio Science*, *39*(1), RS1010. doi: [https://doi.org/10.1029/](https://doi.org/10.1029/2002RS002790)  
326 [2002RS002790](https://doi.org/10.1029/2002RS002790)
- 327 Smith, D. A., Shao, X. M., Holden, D. N., Rhodes, C. T., Brook, M., Krehbiel, P. R., ... Thomas,  
328 R. J. (1999). A distinct class of isolated intracloud lightning discharges and their associated  
329 radio emissions. *Journal of Geophysical Research: Atmospheres*, *104*(D4), 4189-4212. doi:  
330 <https://doi.org/10.1029/1998JD200045>
- 331 Soler, S., Gordillo-Vázquez, F. J., Pérez-Invernón, F. J., Luque, A., Li, D., Neubert, T., ... Østgaard,  
332 N. (2021). Global frequency and geographical distribution of nighttime streamer corona dis-  
333 charges (blues) in thunderclouds. *Geophysical Research Letters*, *48*(18), e2021GL094657. doi:  
334 <https://doi.org/10.1029/2021GL094657>
- 335 Soler, S., Pérez-Invernón, F. J., Gordillo-Vázquez, F. J., Luque, A., Li, D., Malagón-Romero, A., ...  
336 Østgaard, N. (2020). Blue optical observations of narrow bipolar events by ASIM suggest corona  
337 streamer activity in thunderstorms. *Journal of Geophysical Research: Atmospheres*, *125*(16),  
338 e2020JD032708. doi: [10.1029/2020JD032708](https://doi.org/10.1029/2020JD032708)
- 339 Sterpka, C., Dwyer, J., Liu, N., Hare, B. M., Scholten, O., Buitink, S., ... Nelles, A.  
340 (2021). The spontaneous nature of lightning initiation revealed. *Geophysical Research Let-*  
341 *ters*, *48*(23), e2021GL095511. (e2021GL095511 2021GL095511) doi: [https://doi.org/10.1029/](https://doi.org/10.1029/2021GL095511)  
342 [2021GL095511](https://doi.org/10.1029/2021GL095511)
- 343 Stolzenburg, M., Rust, W. D., & Marshall, T. C. (1998). Electrical structure in thunderstorm  
344 convective regions: 3. synthesis. *Journal of Geophysical Research: Atmospheres*, *103*(D12),  
345 14097-14108. doi: <https://doi.org/10.1029/97JD03545>
- 346 Tilles, J. N., Liu, N., Stanley, M. A., Krehbiel, P. R., Rison, W., Stock, M. G., ... Wilson, J. (2019).  
347 Fast negative breakdown in thunderstorms. *Nature communications*, *10*(1), 1–12.
- 348 Uman, M. A., McLain, D. K., & Krider, E. P. (1975). The electromagnetic radiation from a finite  
349 antenna. *American Journal of Physics*, *43*(1), 33-38. doi: [10.1119/1.10027](https://doi.org/10.1119/1.10027)
- 350 Wiens, K. C., Rutledge, S. A., & Tessendorf, S. A. (2005). The 29 June 2000 supercell observed  
351 during steps. part ii: Lightning and charge structure. *Journal of the Atmospheric Sciences*, *62*(12),  
352 4151 - 4177. doi: [10.1175/JAS3615.1](https://doi.org/10.1175/JAS3615.1)
- 353 Wilson, C. T. R. (1956). A Theory of Thundercloud Electricity. *Proceedings of the Royal Society*  
354 *of London. Series A, Mathematical and Physical Sciences*, *236*(1206), 297–317. Retrieved from  
355 <http://www.jstor.org/stable/99960> doi: [10.1098/rspa.1956.0137](https://doi.org/10.1098/rspa.1956.0137)
- 356 Wu, T., Yoshida, S., Akiyama, Y., Stock, M., Ushio, T., & Kawasaki, Z. (2015). Preliminary break-  
357 down of intracloud lightning: Initiation altitude, propagation speed, pulse train characteristics,  
358 and step length estimation. *Journal of Geophysical Research: Atmospheres*, *120*(18), 9071-9086.  
359 doi: <https://doi.org/10.1002/2015JD023546>
- 360 Wu, T., Yoshida, S., Ushio, T., Kawasaki, Z., & Wang, D. (2014). Lightning-initiator type of narrow  
361 bipolar events and their subsequent pulse trains. *Journal of Geophysical Research: Atmospheres*,  
362 *119*(12), 7425-7438. doi: <https://doi.org/10.1002/2014JD021842>
- 363 Zhang, H., Lu, G., Qie, X., Jiang, R., Fan, Y., Tian, Y., ... Feng, G. (2016). Locating narrow bipolar  
364 events with single-station measurement of low-frequency magnetic fields. *Journal of Atmospheric*  
365 *and Solar-Terrestrial Physics*, *143-144*, 88-101. doi: <https://doi.org/10.1016/j.jastp.2016.03.009>

**Table list****Table 1.** The detailed features of the multiple-pulse BLUEs. The detection times of MMIA have been corrected to the source time with respect to the BLUE locations.

ID	MMIA UTC time (source)	Primary BLUE			Subsequent BLUE pulses			Time difference (ms)
		Irradiance ( $\mu W/m^2$ )	Rise time <sup>a</sup> (ms)	Total time duration <sup>b</sup> (ms)	Irradiance ( $\mu W/m^2$ )	Rise time <sup>a</sup> (ms)	Total time duration <sup>b</sup> (ms)	
1	17:50:08.246	4.54	0.18	1.25	2.5	0.05	0.86	3.1
2	17:50:09.645	5.57	0.30	2.25	2.76 <sup>c</sup>	0.58 <sup>c</sup>	1.66 <sup>c</sup>	6.0
3	17:50:19.447	12.42	0.17	1.53	6.08	0.14	1.61	1.7
4	17:50:24.704	10.28	0.79	6.50	3.52	0.14	3.37	9.4
5	17:50:35.617	4.54	0.59	2.45	4.54	0.68	2.64	3.3
6	17:50:43.238	8.69	0.79	3.60	4.54	0.79	3.75	2.6
7	17:50:46.157	10.81	0.06	1.93	3.01	0.22	1.15	7.3
8	17:50:55.181	3.01	0.12	1.19	3.01 <sup>c</sup>	0.41 <sup>c</sup>	2.55 <sup>c</sup>	1.4

<sup>a</sup> Rise time is the time taken for the amplitude of a MMIA photometer signal to rise from 10% to 90%.

<sup>b</sup> Time duration is the time interval for the amplitude of a MMIA photometer signal to rise from 10% and fall to 10%.

<sup>c</sup> The first subsequent BLUE pulse is used to evaluate the rise time and time duration since the photometer signal includes multiple pulses (see Figure S3 and S9 in Supplemental Material for details).

**Table 2.** The inferred features of the multiple-pulse BLUEs. The altitudes ( $H$ ) are estimated using the simplified ray-theory method proposed by (Smith et al., 1999, 2004) based on the ground-based VLF/LF sferics. The depths ( $L$ ) relative to cloud top boundary are evaluated by using the analytical diffusion model in equation (2) in Supplemental Material based on the 337-nm photometer signals of MMIA.

ID	Parameters			NBE			Subsequent pulses	
	Distance $d$ (km)	$N_d$ ( $m^{-3}$ )	$R$ ( $\mu m$ )	337-nm optical energy (J)	Streamer branching events	Altitude $H$ (km)	Depth $L$ (km)	Depth $L$ (km)
1	495	$3 \times 10^8$	20	$1.3 \times 10^3$	$1.0 \times 10^8$	17.68	0.96	0.66
2	494	$2 \times 10^8$	20	$3.7 \times 10^3$	$2.9 \times 10^8$	16.67	1.50	1.74 <sup>a</sup>
3	489	$1 \times 10^8$	20	$6.4 \times 10^3$	$5.0 \times 10^8$	17.03	1.85	1.45
4 <sup>b</sup>	486	-	-	-	-	15.55	-	-
5 <sup>b</sup>	486	-	-	-	-	15.55	-	-
6 <sup>b</sup>	480	-	-	-	-	15.87	-	-
7	482	$1 \times 10^8$	20	$3.8 \times 10^3$	$3.0 \times 10^8$	17.95	1.30	2.79
8 <sup>c</sup>	477	-	-	-	-	17.33	-	-

<sup>a</sup> The first subsequent BLUE pulse is used to obtain the fitting parameters since the photometer signal includes multiple subsequent BLUE pulses (see Figure S3 in Supplemental Material for details).

<sup>b</sup> There is a small pulse on the rising edge of light-curve that distorted the fit process (See Figure S5, S6 and S7 in Supplemental Material for details).

<sup>c</sup> The photometer signal is too noisy to be fitted (See Figure S9 in Supplemental Material for details).

367

**Figures list**

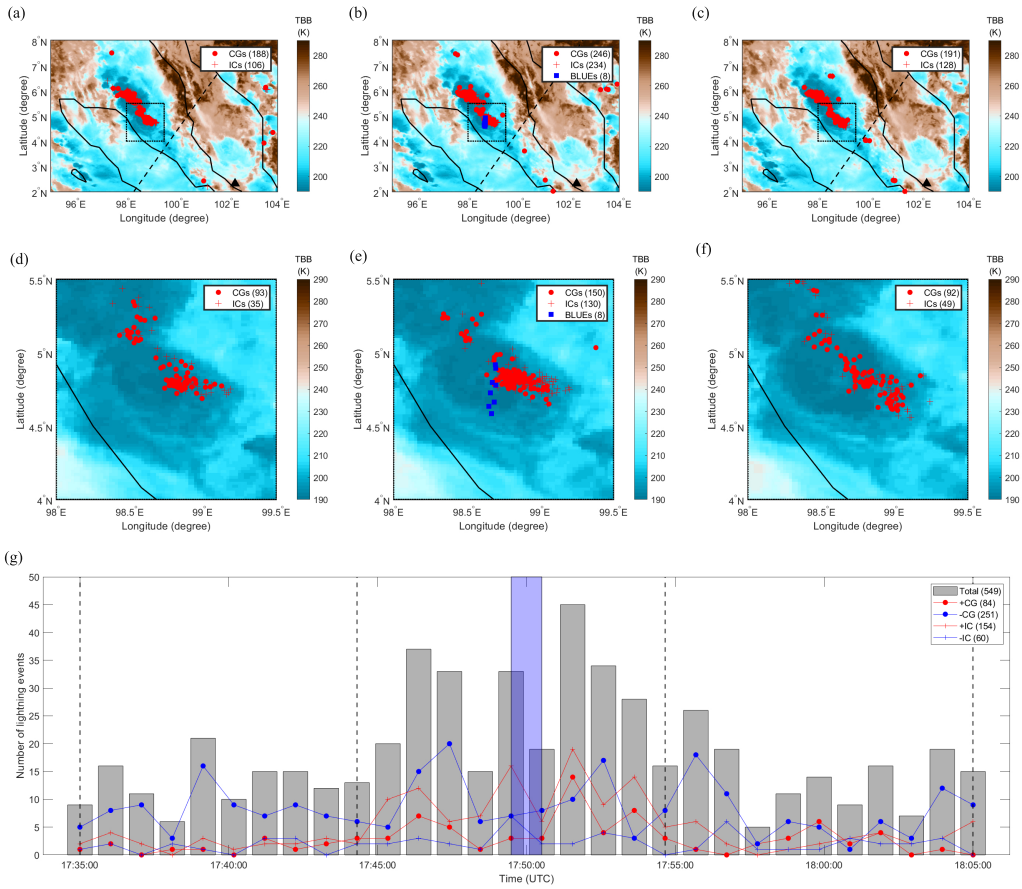


**Figure 1.** Distribution of the intracloud (IC)/cloud-to-ground (CG) lightning with 8 multiple-pulse BLUEs superimposed on the cloud Top Blackbody Brightness temperature (TBB, given in K) in the region of interest and the zoomed-in rectangular region, indicated with the dotted black line, per 10 minutes at time 17:40:00 UTC (a,d), 17:50:00 UTC (b,e), and 18:00:00 UTC (c,f). Numbers of different types of lightning events are shown in (g): positive CGs (+CGs), negative CGs (–CGs), positive ICs (+ICs) and negative ICs (–ICs). The multiple-pulse BLUEs occurred in the time period from 17:50:00 to 17:51:00 UTC marked in blue shaded region in (g). The ground-based VLF/LF sensor at Malaysia is shown as a black triangle in panels (a, b, c). The footprints of ASIM are shown with a black dashed line.

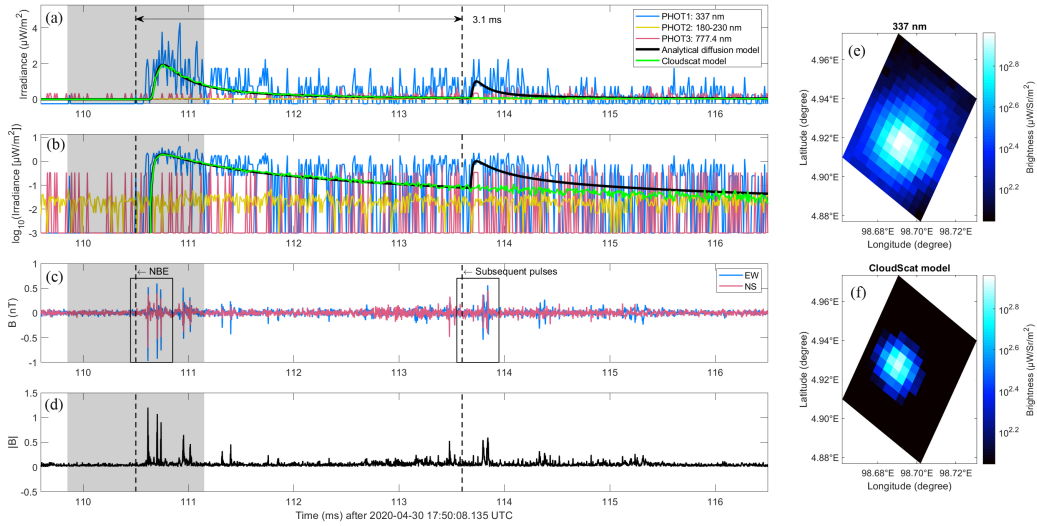


**Figure 2.** Comparison between MMIA photometer irradiance (blue: 337 nm, yellow: 180-230 nm and red: 777.4 nm) and the modeling results of the analytical diffusion model (black) and Cloudscat model (green) on a linear (a) and logarithmic (b) scale, shown together with the North-south and East-west magnetic field components  $B_{NS}$  and  $B_{EW}$  (c) and its norm  $|B| = \sqrt{B_{NS}^2 + B_{EW}^2}$  (d), recorded at the ground-based VLF/LF sensor nearby Malaysia for event 1. Also shown: the image detected by the 337-nm filtered camera of MMIA (e) and the simulated image of the Cloudscat model (f). The start time (corrected to the source time with respect to the locations) for NBE and its subsequent pulses is marked with the dashed black line, within the time difference 3.1 ms with  $\pm 0.65$  ms uncertainty (gray shadowed region).

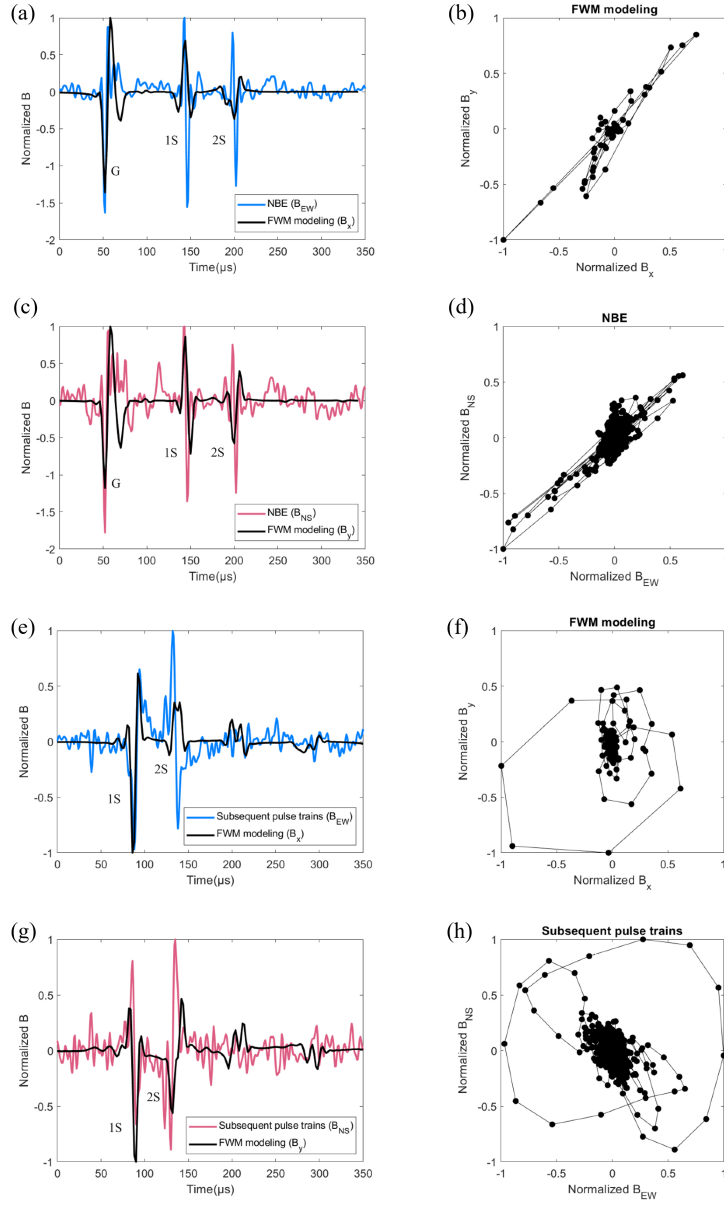


**Figure 3.** Comparison of normalized magnetic field components between the simulation and observation corresponding to the NBE(a,b,c,d) and the subsequent pulses (e,f,g,h) of multiple-pulse BLUE for event 1 (see the black rectangle with the NBE and subsequent pulses labels marked in the figure 2(c)). The magnetic field components of  $B_x$  and  $B_y$  are calculated by the FWM modeling and the North-South and East-West magnetic field components of  $B_{EW}$  and  $B_{NS}$  are measured by the ground-based VLF/LF sensor at Malaysia. The correlation between the different components of the simulated magnetic field ( $B_x$  and  $B_y$ ) and the measured magnetic field components ( $B_{EW}$  and  $B_{NS}$ ) for both NBE (b,d) and the subsequent pulses (f,h) are also shown in the figure. The ground wave and two ionospheric reflected sky waves marked as G, 1S, and 2S.

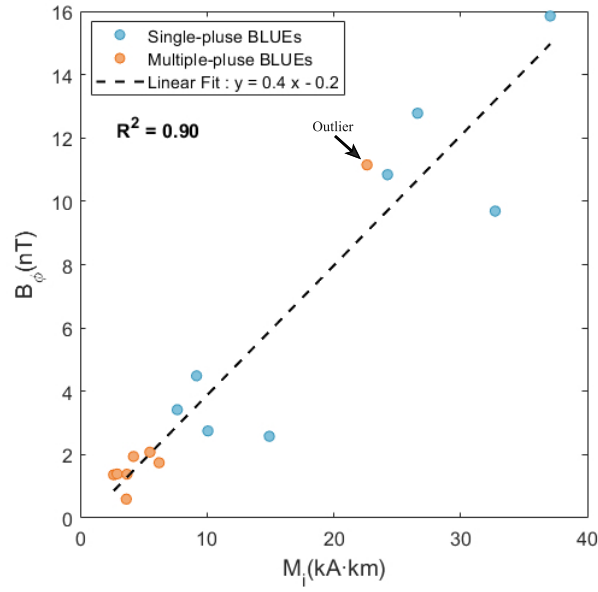


**Figure 4.** Correlation between the amplitude of the azimuthal magnetic field component  $B_{\phi}$  and the inferred current moment  $M_i$  for all the detected BLUES (8 single-pulse BLUES (blue dots) and 8 multiple-pulse BLUES (orange dots)) analyzed in the paper (red dots). The outlier of the multiple-pulse BLUES corresponds to the event with ID 7 in Figure S8 in Supplemental Materials.